Heat Post-Treatment Effect on Optical and Electrical Properties of ZnS Thin Films

Sumit Kumar [1] **, Shruti Bakshi** [1] **, Shilpa Chaudhary** [1] **, Jasmeen Kaur** [1] **,**
Anant Prakash Agrawal [2] **, Suman Rani** [1,*]

1   Department of Physics, School of Chemical Engineering and Physical Sciences, Lovely Professional University, Punjab, India
2   Noida Institute of Engineering and Technology, Gr. Noida
*   Correspondence: suman.rani@lpu.co.in;

Abstract: Heat post-treatment involves subjecting the ZnS thin film to a high-temperature annealing process after deposition on a substrate. The primary goal of heat post-treatment is to improve the crystalline structure of the ZnS film, which can significantly impact its electrical and optical properties. Zinc sulfide (ZnS) films are broadly utilized in photovoltaic instruments because of their versatile properties. In this study, we deposited ZnS films on glass substrates using spin coating at a temperature of 500°C and investigated the impact of film thickness on their optical and electrical characteristics. We employed various characterization techniques such as UV-visible (UV-V) spectroscopy, X-ray diffraction (XRD), and two-point techniques to analyze the electrical and optical properties of ZnS thin films. During the heat treatment, the ZnS film is annealed, which promotes the formation of well-defined crystalline grains and reduces the number of defects in the film. A thin Zinc Sulfide film shows the film's thickness from 445 nm to 1778 nm. The electrical resistivity of the films was also measured and found to be in the range of 8.34×10^5 to 56.71×10^5 Ohm-m. Our results demonstrate the significant impact of film thickness on the electrical and optical properties of ZnS films, which can be useful in developing photovoltaic devices.

Keywords: ZnS; post heat treatment; transparent conducting material; thin films.

1. Introduction

Zinc sulfide (ZnS) is a versatile material with many applications, including optoelectronics, solar cells, and transparent conductive coatings. As a transparent conducting material, ZnS has several advantages over other normally utilized materials, such as fluorine-doped tin oxide (FTO) and indium tin oxide (ITO) [1]. One of the main advantages of ZnS is its high transparency in the visible region of the spectrum, making it suitable for use in transparent conductive coatings for displays and touchscreens [2,3]. Additionally, ZnS has a high refractive index, which can be used to enhance the performance of light-emitting devices and solar cells [4]. ZnS also has good electrical conductivity, making it a viable alternative to ITO and FTO for transparent conducting applications. ZnS has been shown to exhibit better conductivity than ITO in certain situations, particularly at high temperatures. Another advantage of ZnS is its abundance and low cost [5]. Unlike indium, a rare and expensive element, zinc is readily available and relatively inexpensive. This makes ZnS a more sustainable and cost-effective option for transparent conductive applications. Overall, the

unique combination of high transparency, high refractive index, good electrical conductivity, and low cost make ZnS a promising material for various transparent conductive applications [6].

ZnS has a band gap of around 3.7 eV and is optically transparent [7,8]. It is an inexpensive, environmentally friendly substance with superior mechanical features, perfect hardness, and fracture strength [9]. Zincblende (ZB) and wurtzite are the two crystalline forms of ZnS [10]. The fact that it is transparent throughout such a broad energy range, from visible wavelengths to slightly over 12 micrometers, makes it the perfect material for various devices, including sensors, light-emitting diodes[LED], solar cells, and liquid crystal displays [11].

Overall, this study contributes to the knowledge of ZnS's optical and electrical properties, providing insights for developing novel materials and devices with practical applications.

2. Materials and Methods

The sol-gel technique is used to create the ZnS solution. The starting material used to prepare the sol is zinc acetate dehydrated salt as a zinc precursor, thiourea as a sulfide precursor, acetone as a solvent, distilled water, isopropanol, and monoethanolamine (MEA) as a stabilizer. Firstly, we dissolved 0.439 grams of 0.1 M zinc acetate dehydrate (20 ml) in propanol-1 to yield 0.002 mol Zn, regardless of the final solution volume. We then stirred the solutions at 50°C to 60°C and added 10 drops of MEA after 30 minutes of stirring. We added a NaOH solution to attain a pH level of 12, producing transparent and uniform solutions. We added 20 ml of 0.3 M thiourea to the solutions, further stirred at 50°C to 60°C. We utilized the same amount of thiourea (0.4536 grams) in each precursor solution. Finally, we stirred the prepared sols under magnetic stirring at a temperature of 50°C to 60°C for two hours.

The 2×2 cm glass substrates underwent a cleaning procedure that included soaking them in acetone for 24 hours, washing them with detergent, rinsing them with distilled water, and allowing them to air dry. The polished surface of the substrate adheres evenly over its surface. Thin ZnS films were deposited on the cleaned glassware using a sol-gel spin coating with a spin speed of 3000 rpm. The spin coating process was repeated 6, 8, 10, and 12 times, resulting in samples with 6, 8, 10, and 12-layer films with thicknesses of 445, 889, 1374, and 1778 nm (S6, S8, S10, and S12), respectively. Each layer of ZnS consisted of 3 drops of the ZnS solution. To crystallize the films, the S6, S8, S10, and S12 layer samples were placed in a furnace and subjected to post-heating for 5 hours at various temperatures, 300°C to500°C.

3. Results and Discussion

3.1. XRD Pattern.

Figure 1 shows the X-ray diffraction graph of the 8-layer films (S8) that were formed on a glass substrate at annealing temperatures of 300°C, 400°C, and 500°C. Thin films were examined for phase purity and crystal structure using an XPERT-PRO diffractometer with a Cu-K radiation source at 20-60°C. The XRD pattern of the artificial ZnS layer is displayed in Figure 1. The diffraction data of ZnS was consistent with the JCPDS data (JCPDS 72-0163).
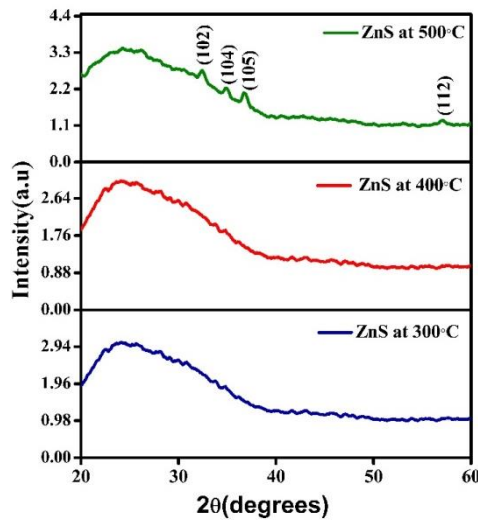
Figure 1. X-ray diffraction pattern of S8 layers(thickness 889 nm).

The hexagonal wurtzite structure was observed, which exhibited three major peaks at (102), (104), and (105) and closely matched the literature [12,13].

$$D = \frac{0.89\lambda}{\beta cos\theta} \qquad (1)$$

The Debye-Scherrer equation (1) [14], where λ, θ, and β stand for the Cu-K radiation wavelength, Braggs angle, and full width at half maximum of the diffraction plane respectively, were utilized to estimate the average particle size (D) of the synthesized ZnS nanoparticles [15]. The average crystallite size of the ZnS nanoparticles was determined to be between 32.41 and 32.46 nm. The XRD examination of the coated samples with 8 layers indicated a higher level of crystallinity in the films, which revealed that all significant reflection peaks got narrower and sharper with increased intensity. The ZnS thin film crystallinity rose when the annealing temperature was raised, peaking at 500°C. No new reflections arose even though the strength of the reflections generally dropped as the annealing temperature increased, proving that no new phases were created.

3.2. UV-visible spectrosocpy.

The optical characteristics of the ZnS thin films formed on glass substrate layers (S6, S8, S10, S12) were investigated using a UV-visible spectrophotometer. The optical spectra of the films annealed at 500°C were obtained by a spectrophotometer, as shown in Figure 2 and 3. The transmittance of all samples was found to increase in 400 nm–600 nm as shown in figure 2(b), with a transmission greater than ~90% observed for a wavelength of 400 nm [16].

Among the samples, S8 exhibited the highest transmission of 99.03% in 400–600 nm, followed by S6 at approximately 95% and S12 at about 91.98%. On the other hand, S10 had the lowest transmittance value of ~65.21%. The thickness of the films significantly affected their optical transmittance, as shown in Figure 2b. The good transmittance observed in the films to the improved crystal structure of the ZnS thin films resulting from the annealing process, as shown by the X-ray diffraction spectra [17,18].
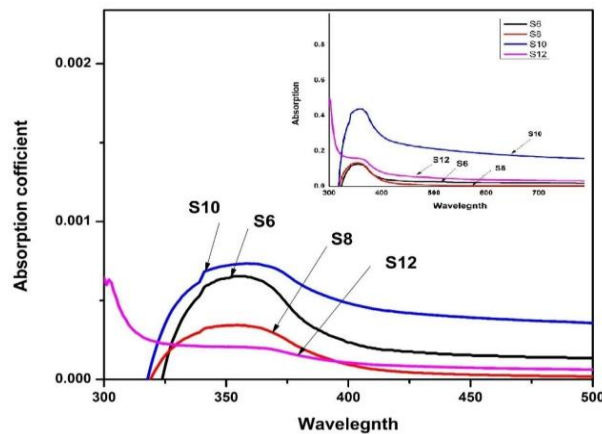
(a)   **(b)**
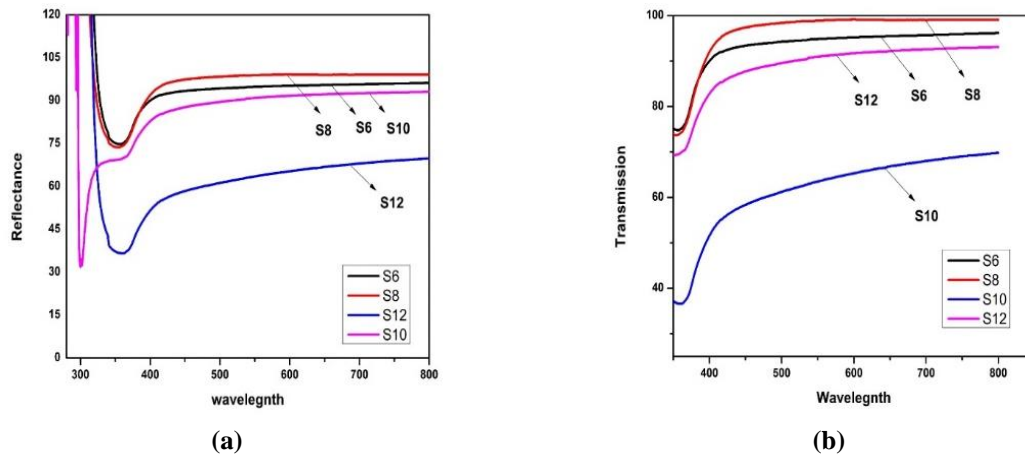
Figure 2. (a) Refection spectra of ZnS with respect to the thickness of thin films; **(b)** Transmission spectra of ZnS with respect to the thickness of thin films.

The value of the absorption coefficient (α) is calculated by using

$$\alpha = \frac{2.303A}{d} \qquad (2)$$

where the 'd' is the thickness of the thin film measured by the weight method.

Figure 3. Absorption coefficient of S6, S8, S10 and S12 layers.

Due to its wide bandgap, ZnS exhibits strong absorption in the ultraviolet region. The thickness of a ZnS layer can significantly affect its UV absorption properties [19]. Figure 2 shows that the thickness absorption increases towards shorter wavelengths, resulting in a blue shift in the absorption spectrum. In thin ZnS films, the confinement of the excitons becomes more pronounced due to the reduced dimensionality of the material. This results in a higher energy level for the excitons, corresponding to a shorter wavelength of light absorbed. As the thickness of the ZnS film increases, the confinement effect diminishes. Therefore, the thickness of the ZnS layer must be carefully optimized to achieve the desired UV absorption properties for specific applications. For example, in optoelectronic devices such as photodetectors, a thin ZnS layer is desirable to achieve high UV sensitivity. On the other hand, in UV-blocking applications, a thicker ZnS layer may be required to provide effective UV absorption. Maximum absorption takes place at a thickness of 1373 nm.

The optical absorption coefficient in the visible range for the deposited films was investigated and is shown in Figure 3. The absorption coefficient values were found to be quite low ($\alpha > 3$ cm^{-1}). Among the samples, the S10 film had the highest absorption coefficient value of 7.41 cm-1, while the S12 film had the lowest value of 1.96 cm^{-1}. The order of the absorption coefficient (α) for the Zinc Sulfide thin films is S10 > S6 > S8 > S12.

The extinction coefficient(K) of ZnS thin films from the α is calculated by using equation (3)

$$K = \frac{\lambda\alpha}{4\Pi} \qquad (3)$$

Figure 4 illustrates the rapid increase in the extinction coefficient values of S6, S8, S10, and S12 films from the UV to the near-visible region (320–360 nm), indicating a slight absorption of ZnS in the visible spectrum. However, the annealed ZnS thin films exhibit shallow extinction coefficient values (around 0.002) in the visible and near-infrared range, indicating a smooth surface [20]. The order of the extinction coefficient for the thin films is S6 > S10 > S8 > S12. The attenuation or extinction coefficient (k) of ZnS thin films depends on the wavelength and material properties [21].
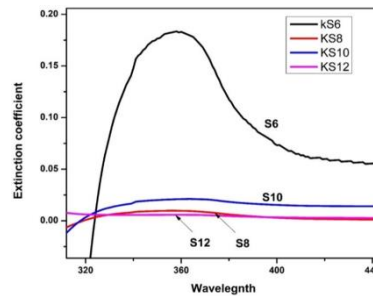
Figure 4. Extinction coefficient values of ZnS S6, S8, S10, and S12 layers with respect to wavelength.

To investigate the optical properties of ZnS thin films, the refractive index was calculated by equation (4)

$$\eta = n + ik \qquad (4)$$

where the refractive index (n) is given by equation (5) [22,23]

$$n = \frac{1+\sqrt{R}}{1-\sqrt{R}} \qquad (5)$$

where R is the reflection coefficient.

The wavelength-dependent refractive index of ZnS thin films (S6, S8, S10, and S12) at an annealing temperature of 500°C is presented in Figure 5. Thin films exhibit uniform appearance and performance, and a decreasing trend in refractive index is seen as the wavelength increases from 350 to 800 nm.
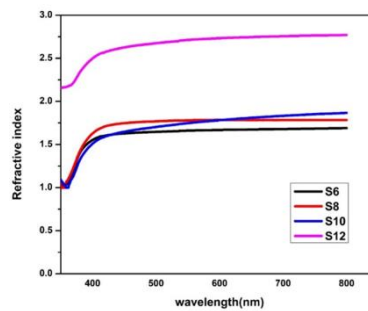
Figure 5. Refractive index for ZnS thin films of S6, S8, S10, and S12 layers.

The energy band gap (Eg) was calculated from Tauc's relation and was estimated by using relation (6) [24,25]

$$\alpha h\vartheta = A(h\vartheta - E_g)^n \qquad (6)$$

where absorption coefficient (α), the energy of the photon (hv), and an energy-independent constant (A). The Exponent value (n) depends on the type of transition and can be 2, 1/2, or 3. For a direct band gap value put n=1/2 in equation 6 which result in equation 7 and 8 respectively.

$$\alpha h\vartheta = A(h\vartheta - E_g)^{1/2} \qquad (7)$$

$$(h\vartheta\alpha)^2 = A(h\vartheta - E_g) \qquad (8)$$

The optical band gap of ZnS films is calculated by extrapolating the linear portion of the Tauc's plot to 0 absorption (h=0), which ends up in the graph among $(\alpha h\upsilon)^2$ and photon strength ($h\upsilon$), which is displayed in Figure 6 [26].
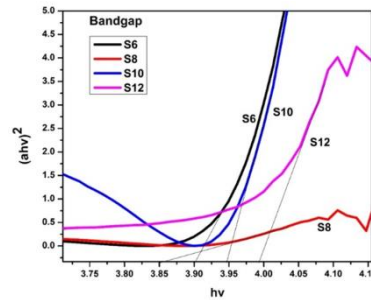
Figure 6. Graph of optical band gap for different thicknesses of ZnS thin films.

The thickness of the thin films S6, S8, S10, and S12 is calculated using the weight method, and the bandgap and refractive indexes of the respective thin films are shown in Table 1.

Table 1. Summaies the thickness, optical bandgap, and refractive index of ZnS thin films.

Sample	Thickness (nm)	Bandgap (eV)	Refractive index
S6	444.54	3.90	1.06
S8	889.28	3.85	1.08
S10	1373.82	3.94	1.07
S12	1778.36	3.98	2.13

3.3. Electrical properties of ZnS thin films.

The two-wire sensing method, called the two-point probe, is commonly used to characterize semiconductor materials [27]. It is often employed to determine the resistivity of films. The fundamental electrical property classifies any material as a conductor, insulator, or semiconductor is its electrical impedance (ρ), making it a crucial characteristic to measure or evaluate when exploring new materials [28].

Using the Old Jandel two-point probe setup of the SES instrument, the configuration was used to look into the films created during this research. A silver paste has been used to ensure satisfactory ohmic contact with the film. Investigations were done on the resistivity and conductivity values for films S6, S8, S10, and S12. The relation used to measure the resistivity(ρ) is described in relation 9 [29].

$$\rho = \frac{\Pi t \upsilon}{ln\ 2I} = 4.532\frac{t\upsilon}{I} \qquad (9)$$

Where 'V' is the voltage applied, 'I' is the current, and 't' is the thickness of ZnS thin films. The sheet resistance (Rs), resistivity(ρ) and conductivity (σ) of ZnS thin films were calculated by using equations 10,11 and 12 respectively. The Rs value was determined by calculating the slope of the voltage versus current graph shown in Figure 7 obtained from the two-point probe measurements. Thus, the two-point probe setup determined the sheet resistance for the S6, S8, S10, and S12 thin films.

$$R_s = 4.532\frac{V}{I} \qquad (10)$$

$$\rho = R_s \times t \qquad (11)$$

electrical resistivity was assumed to be the reciprocal of the electrical conductivity(σ) as given in the Eq. (10)

$$\sigma = \frac{1}{\rho} \qquad (12)$$

The graph in Figure 7 exhibits smooth and ohmic behavior, indicating that the films are semiconducting. They were increasing the electrode voltage, which resulted in a corresponding increase in the current flowing through the films. The observed increase in forward current at all voltages suggests that the films have higher conductivity, which has the potential to enhance the efficiency of solar cell manufacturing [30]. The electrical conductivity (σ), resistivity (ρ), and thickness (t) values of the deposited ZnS films are presented in Figure 8.
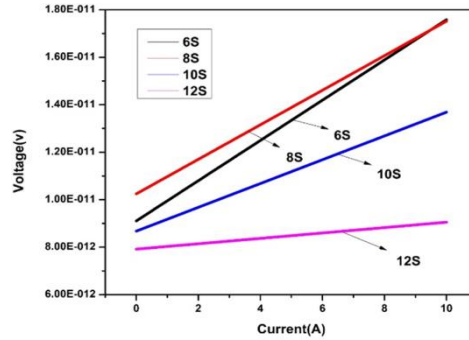
Figure 7. Current-voltage characteristics of ZnS thin films at different thicknesses.

Figure 8 illustrates the electrical resistivity and conductivity changes across the different samples. It can be observed that the electrical conductivity increased from S6 to S12, while the electrical resistivity increased in the same order. Interestingly, the opposite pattern was observed for the electrical conductivity when compared to the resistivity. The decrease in resistivity of the thin films can be attributed to the increase in pairs of electrons and holes generated due to the introduction of zinc into the ZnS system.
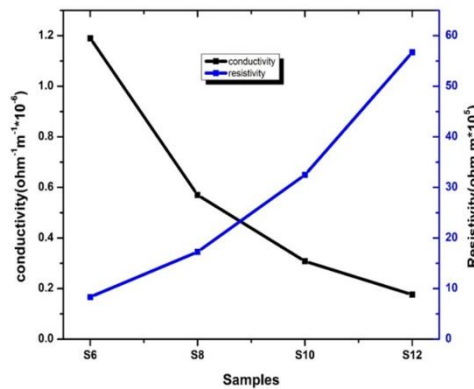
Figure 8. Variation of resistivity and conductivity with different layers of thin films.

4. Conclusions

We deposited ZnS films on glass substrates using spin coating at a temperature of 500°C and investigated the impact of film thickness on their optical and electrical characteristics. The XRD analysis revealed the formation of hexagonal-structured zinc sulfide with a crystallite size ranging from 32.41-32.46 nm. The transmittance (%) of the ZnS thin lies in the visible region (400-800 nm) varied from 60-95% for different thicknesses of the films. The direct band gap energy of the ZnS thin films ranged from 3.85 to 3.98 eV. The thickness of the films varied from 445 nm to 1778 nm. The electrical resistivity of the films was also measured and found to be in the range of 8.34×10^5 to 56.71×10^5 Ohm-m. Our results demonstrate the significant impact of film thickness on the electrical and optical properties of ZnS films, which can be useful in developing photovoltaic devices.

Funding

Acknowledgments

Conflicts of Interest

The authors declare no conflict of interest.

References

1. Benyahia, K.; Djeffal, F.; Ferhati, H.; Benhaya, A.; Bendjerad, A.; Djaballah, Y.; Martin, N. Microstructured ZnO-ZnS composite for earth-abundant photovoltaics: Elaboration, surface analysis and enhanced optical performances. *Sol. Energy* **2021**, *218*, 312-319, http://doi.org/10.1016/j.solener.2021.02.057.

2. Kaur, N.; Kaur, S.; Singh, J.; Rawat, M. A Review on Zinc Sulphide Nanoparticles: From Synthesis, Properties to Applications. *J. Bioelectron. Nanotechnol.* **2016**, *1*, 5, http://doi.org/10.13188/2475-224X.1000006.

3. Kumar, V.; Saroja, M.; Venkatachalam, M.; Balachander, M.; Shankar, S. Synthesis and Characterization of ZnS, MZS and CZS films prepared by Sol-Gel Spin Coating method. *Int. J. Chem. Concepts* **2017**, *3*, 150-154.

4. Lee, S.; Kim, J.; Lee, H. Substrate Dependence of CdSe/ZnS Quantum-Dot Light-Emitting Diodes: A Comparative Study between Rigid Glass and Flexible Plastic Substrates. *Nanomaterials* **2023**, *13*, 1780, http://doi.org/10.3390/nano13111780.

5. Cheng, W.; Di, H.; Shi, Z.; Zhang, D. Synthesis of ZnS/CoS/CoS$_2$@N-doped carbon nanoparticles derived from metal-organic frameworks via spray pyrolysis as anode for lithium-ion battery. *J. Alloys Compd.* **2020**, *831*, 154607, http://doi.org/10.1016/j.jallcom.2020.154607.

6. Qing, X.; Zhang, C.; Gong, J.; Chen, S. Ab initio study of photoelectric properties in ZnO transparent conductive oxide. *Vacuum* **2021**, *191*, 110391, http://doi.org/10.1016/j.vacuum.2021.110391.

7. Sayeed, M.A.; Rouf, H.K.; Hussain, K.M.A. Doping and annealing effects on structural, optical and electrical characteristics of Sn-doped ZnS thin film. *Mater. Res. Express* **2021**, *8*, 086401, http://doi.org/10.1088/2053-1591/ac1964.

8. Khodamorady, M.; Bahrami, K. A novel ZnS-CdS nanocomposite as a visible active photocatalyst for degradation of synthetic and real wastewaters. *Sci. Rep.* **2023**, *13*, 2177, http://doi.org/10.1038/s41598-023-28725-7.

9. Sundhar, A. Development of ZnS thin film with Co, Cu, and Ag doping using SILAR method. *Mater. Today Proc.* **2022**, *48*, 377-381, http://doi.org/10.1016/j.matpr.2020.09.550.

10. Jonnalagadda, M.; Prasad, V.B.; Raghu, A.V. Synthesis of composite nanopowder through Mn doped ZnS-CdS systems and its structural, optical properties. *J. Mol. Struct.* **2021**, *1230*, 129875, http://doi.org/10.1016/j.molstruc.2021.129875.

11. Shkir, M.; Palanivel, B.; Chandekar, K.V.; Khan, A.; El-Toni, A.M.; Ansari, A.A.; AlFaify, S. Microwave-assisted synthesis of Cu doped PbS nanostructures with enhanced dielectric and electrical properties for optoelectronic applications. *Mater. Sci. Eng. B* **2021**, *271*, 115268, http://doi.org/10.1016/j.mseb.2021.115268.

12. Ruffner, J.A.; Himel, M.D.; Mizrahi, V.; Stegeman, G.I.; Gibson, U.J. Effects of low substrate temperature and ion assisted deposition on composition, optical properties, and stress of ZnS thin films. *Appl. Opt.* **1989**, *28*, 5209-5214, http://doi.org/10.1364/AO.28.005209.

13. Gangopadhyay, U.; Kim, K.; Dhungel, S.K.; Saha, H.; Yi, J. Application of CBD-Zinc Sulphide Film as an Antireflection Coating on Very Large Area Multicrystalline Silicon Solar Cell. *Adv. OptoElectron.* **2007**, *2007*, 018619, http://doi.org/10.1155/2007/18619.

14. Bakshi, S.; Rani, S.; Kaur, P. Down conversions luminescent properties of Eu doped SrTiO$_3$. In 3rd International Conference on Recent Advances in Fundamental and Applied Sciences (RAFAS 2021), Online, 24/06/2021-26/06/2021; IOP Publishing Ltd, **2022**, 2267, 01204, http://doi.org/10.1088/1742-6596/2267/1/012042.

15. Han, Y.; Hamada, M.; Chang, I.-Y.; Hyeon-Deuk, K.; Kobori, Y.; Kobayashi, Y. Fast T-Type Photochromism of Colloidal Cu-Doped ZnS Nanocrystals. *J. Am. Chem. Soc.* **2021**, *143*, 2239-2249, http://doi.org/10.1021/jacs.0c10236.

16. Tounsi, A.; Khalfi, R.; Talantikite-Touati, D.; Merzouk, H.; Souici, A. Characterization of cerium-doped zinc sulfide thin films synthesized by sol–gel method. *Appl. Phys. A* **2022**, *128*, 280, http://doi.org/10.1007/s00339-022-05409-z.

17. Noikaew, B.; Chinvetkitvanich, P.; Sripichai, I.; Chityuttakan, C. The Influence of Growth Conditions on the Chemical Bath Deposited ZnS Thin Films. *J. Met. Mater. Miner.* **2008**, *18*, 49-52.

18. Lakshmi, P.V.B.; Raj, K.S.; Ramachandran, K. Synthesis and characterization of nano ZnS doped with Mn. *Cryst. Res. Technol.* **2009**, *44*, 153-158, http://doi.org/10.1002/crat.200800271.

19. Çam, Ş.U.; Serin, T.; Yazıcı, A.N. Effect of Sn doping concentration on structural, optical, and electrical properties of ZnS/p-Si (111) diodes fabricated by sol-gel dip-coating method. *Mater. Sci. Semicond. Process.* **2021**, *127*, 105693, http://doi.org/10.1016/j.mssp.2021.105693.

20. El-Desoky, M.M.; Ali, M.A.; Afifi, G.; Imam, H. Annealing effects on the structural and optical properties of growth ZnO thin films fabricated by pulsed laser deposition (PLD). *J. Mater. Sci. Mater. Electron.* **2014**, *25*, 5071-5077, http://doi.org/10.1007/s10854-014-2273-8.

21. Thakur, Y.S.; Acharya, A.D.; Sharma, S.; Bhawna. Reinforcement of V$_2$O$_5$ nanoparticle in polyaniline to improve the optical and UV-shielding properties. *Results Opt.* **2023**, *11*, 100400, http://doi.org/10.1016/j.rio.2023.100400.

22. Sanjeev, S.; Kekuda, D. Effect of annealing temperature on the structural and optical properties of zinc oxide (ZnO) thin films prepared by spin coating process. In IOP Conference Series: Materials Science and Engineering, Kerala, India, 10-14 June 2012; IOP Publishing Ltd, **2015**, *73*, 012149, http://doi.org/10.1088/1757-899X/73/1/012149.

23. Hussein, H.F.; Shabeeb, G.M.; Hashim, S.S.; Preparation ZnO Thin Film by using Sol-gel-processed and determination of thickness and study optical properties. *J. Mater. Environ. Sci.* **2011**, *2*, 423-426.

24. Tauc, J. Band tails in amorphous semiconductors. *J. Non-Cryst. Solids* **1987**, *97*, 149-154, http://doi.org/10.1016/0022-3093(87)90035-4.

25. Jebathew, A.J.; Karunakaran, M.; Ade, R.; Jayram, N.D.; Ganesh, V.; Bitla, Y.; Vinoth, S.; Algarni, H.; Yahia, I.S. Optical manipulation of nebulizer spray pyrolysed ZnS thin films for photodetector applications: Effect of Al, Sn and Sb doping. *Opt. Mater.* **2021**, *117*, 111177, http://doi.org/10.1016/j.optmat.2021.111177.

26. Emegha, J.O.; Okafor, C.M.; Uukhurebor, K.E. Optical Properties of Copper-Zinc Sulphide Network from Mixed Single Solid Source Precursors of Copper and Zinc Dithiocarbamates. *Walailak J. Sci. Technol.* **2021**, *18*, 9535, http://doi.org/10.48048/wjst.2021.9535.

27. Chandra, N.; Sharma, V.; Chung, G.Y.; Schroder, D.K.; Four-point probe characterization of 4H silicon carbide. *Solid-State Electron.* **2011**, *64*, 73-77, http://doi.org/10.1016/j.sse.2011.07.004.

28. Barquinha, P.M.C. Transparent Oxide Thin-Film Transistors: production, characterization, and integration. Degree of Doctor of Philosophy in Nanotechnologies and Nanosciences, Universidade Nova de Ciências e Tecnologia, Lisboa, Portugal, **2010.**

29. Emegha, J.O.; Olofinjana, B.; Ukhurebor, K.E.; Adegbite, J.T.; Eleruja, M.A. Electrical Properties of Semiconducting Copper Zinc Sulphide Thin Films. *Curr. Appl. Sci. Technol.* **2022**, *22*, 10-55003, http://doi.org/10.55003/cast.2022.01.22.003.

30. Forouhi, A.R.; Bloomer, I. Optical dispersion relations for amorphous semiconductors and amorphous dielectrics. *Phys. Rev. B* **1986**, *34*, 7018, http://doi.org/10.1103/PhysRevB.34.7018.